Research Square

Preprints are preliminary reports that have not undergone peer review.
They should not be considered conclusive, used to inform clinical practice,
or referenced by the media as validated information.

Comparison of phosphate adsorption on kaolinite, illite and montmorillonite by surface complexation modelling

Ying Huang
Southwest University
Jing Liu
liujing-vip@163.com

Southwest University https://orcid.org/0000-0002-1187-6652

Research Article

Keywords: Clay minerals, Phosphate, Adsorption, Surface complexation model

Posted Date: November 4th, 2026

DOI: https://doi.org/10.21203/rs.3.rs-11189407/v1

License: This work is licensed under a Creative Commons Attribution 4.0 International License.
Read Full License

Comparison of phosphate adsorption on kaolinite, illite and montmorillonite by surface complexation modelling

Ying Huang [a],Jing Liu[a,*]

[a]College of Resources and Environment, Southwest University, Chongqing, 400716, China. Tel: +86-19132099507

[*]Corresponding author: Jing Liu

E-mail: liujing-vip@163.com

Tel: +86(023)-68251249

Abstract

Kaolinite, montmorillonite, and illite are representative silicate minerals that play important roles in controlling the fate and mobility of phosphorus in soils. In this study, phosphate adsorption on these minerals was described using two surface complexation models, namely the Constant Capacitance Model (CCM) and the Triple Layer Model (TLM). The determination of surface site densities and surface complexation constants was evaluated and compared. Compared with the CCM, the TLM provided a better description of phosphate adsorption envelopes under different ionic strength conditions. In the TLM, the optimized equilibrium constants for the $AlHPO_4^-$, $SiOH_2^+$–PO_4^{3-}, and $AlPO_4^{2-}$ surface complexes were 24.53, 18.60, and 17.44 for kaolinite, 23.68, 17.83, and 17.56 for montmorillonite, and 23.09, 19.51, and 17.23 for illite, respectively. After normalization to mineral mass, the maximum phosphate adsorption capacities were 3.81×10^{-6}, 6.23×10^{-6}, and 1.88×10^{-6} mol/g for kaolinite, montmorillonite, and illite at same initial concentration 8.40×10^{-5} mol/L, respectively, indicating that montmorillonite exhibited the highest adsorption capacity, whereas kaolinite and illite

* Corresponding author: liujing-vip@163.com (LIU JING)

reached approximately 61.1% and 30.1% of that of montmorillonite, respectively. ATR-FTIR spectra showed characteristic phosphate bands at 650, 960, 1027, and 1100 cm^{-1}, corresponding to the ν_4, ν_1, and ν_3 vibrational modes of phosphate. The spectroscopic results indicated that phosphate was adsorbed in similar surface species on all three minerals. Adsorption-envelope similarity analysis revealed that kaolinite and illite exhibited more comparable phosphate adsorption behaviors, whereas montmorillonite showed distinctly different adsorption characteristics. These findings highlight the importance of identifying and quantifying clay mineral compositions in soils and contribute to the development of consistent and realistic protocols for modelling ion adsorption reactions on soil minerals and soils.

Keywords: Clay minerals, Phosphate, Adsorption, Surface complexation model

1. Introduction

Both organic and inorganic phosphorus (P) widely occurs in soils environment (Berg and Joern 2006). It is an essential nutrient regulating plant growth and agricultural productivity. Organic phosphorus mainly consists of inositol phosphates, nucleic acids, and phospholipids, accounting for approximately 5-75% of the total soil phosphorus pool (Dalal 1977; Levesque and Schnitzer 1967). A significant proportion of organic P can be stabilized through interactions with soil organic matter and microbial biomass, thereby contributing to long-term phosphorus cycling in soils (Stewart and Tiessen 1987; Perrott et al. 1990). In contrast, inorganic phosphorus is generally regarded as the dominant form controlling phosphorus availability and mobility in most agricultural soils. The fate of inorganic phosphate is strongly influenced by adsorption and desorption reactions occurring at mineral surfaces (Brady and Weil 2002). These processes regulate phosphate retention, transport, and bioavailability.

Clay minerals represent one of the most abundant and reactive components owing to their large specific surface areas, variable surface charges, and diverse surface functional groups (Schoonheydt et al. 2018). Kaolinite, montmorillonite, and illite are among the most common clay minerals found in natural soils and sediments (Miranda-Trevino and Coles 2003; Abollino et al. 2008). Their structural differences and surface chemical properties can substantially affect phosphate adsorption behavior, including adsorption capacity, pH dependence, and adsorption mechanisms. Consequently, understanding the interactions between phosphate and representative clay minerals is essential for elucidating phosphorus retention processes in soils and predicting phosphorus mobility under varying environmental conditions.

Surface complexation modelling (SCM) is an important tool for understanding binding mode of adsorbing ions as function of the local conditions (pH) based on a thermodynamic basis (Dzombak and Morel 1990; Davis and Kent 1990; Goldberg and Criscenti 2008). It could build a link microscopic adsorption and preferably the parameters. These parameters are highly valuable for predicting the adsorption behavior of soils containing the same dominant minerals (Gu 2006; Gauthier 2011; Goldberg 2014). The Constant Capacitance Model (CCM), the Diffuse layer modeling (DLM), the Triple Layer Model (TLM) and the Charge Distribution Multi-site Complexation model (CD-MUSIC) are the common four SCM developed to describe the adsorption of phosphate. Goldberg firstly described phosphate adsorption on iron oxides and clay minerals, and claimed that the surface AlOH group is more important than SiOH (Goldberg 1985). The main adsorbed species of phosphate are $\equiv SH_2PO_4$, $\equiv SHPO_4^-$ and $\equiv SPO_4^{2-}$. The surface protonation and deprotonation constants of kaolinite are 4.61 and −6.68, respectively. These parameters have been shown to effectively simulate the adsorption of heavy metals, including Cd, Cu, Ni, Zn, and Pb, onto kaolinite. Using the

Constant Capacitance Model (CCM), Manning and Goldberg (1996) fitted phosphate adsorption on illite and kaolinite, obtaining surface complexation constants of 30.02, 25.10, and 15.74 for illite, and 31.72, 24.68, and 17.17 for kaolinite. However, comparative studies on phosphate adsorption and its surface complexation modeling among typical clay minerals remain limited. In this study, phosphate adsorption envelopes of kaolinite, montmorillonite, and illite were investigated under different ionic strength conditions. The CCM and TLM were employed to compare their adsorption behaviors, while ATR-FTIR spectroscopy was used to elucidate the underlying surface adsorption mechanisms. Differences in phosphate adsorption among the three clay minerals were evaluated through adsorption-envelope comparisons, providing useful insights for soil chemistry studies and reactive transport modeling.

2. Materials and methods

2.1 Acid-Washed and Ion-Exchanged Kaolinite, illite and montmorillonite

Kaolinite, illite and montmorillonite were collected from Fuzhou city of Fuzhou province, Shijiazhuang city of Hebei province and Chifeng city of Mongolia province, China. They were crushed and sieved to 200 meshes (75 μm). X-ray diffraction (XRD) confirmed the corresponding mineralogical identification of the samples.

5g kaolinite, illite and montmorillonite were mixed with 15 mL of 0.1 M KOH solution at a solid-to-liquid ratio of 1:3 and shaken at 150 rpm for 0.5 h to remove impurities from them respectively. These particles smaller than 2 μm were obtained by gradient centrifugation (800 rpm for 3 min). The upper suspension was transferred into another centrifuge tube, while the sediment remaining at the bottom of the original tube was discarded. The sample slurries was further centrifuged at 8000 rpm for 5 min, and the supernatant was discarded. Subsequently, 15 mL of 1 M KCl solution adjusted to pH 3 (adjusted by 0.1 M HCl) was added into the centrifuge tube, followed by re-dispersion

using a homogenizer. The suspension was then centrifuged again at 8000 rpm for 5 min, and the supernatant was removed. Fresh 15 mL of pH 3, 1 M KCl solution was added again, re-homogenized, and centrifuged at 8000 rpm for 5 min again. This procedure was repeated four times in total. Subsequently, 15 mL of 0.01 M KCl solution was added to each centrifuge tube, and the samples was homogenized and equilibrated at 25 °C for 24 h. The suspension was then centrifuged at 8000 rpm. Finally, the obtained samples were freeze-dried and stored in a desiccator for subsequent experiments. The above procedures were repeated multiple times to obtain a sufficient amount of samples for subsequent experiments.

2.2 Potentiometric titrations

Various amounts of clay and 40 mL 0.01M KCl background electrolyte were added to the vessel and purged with high pure argon for two hours. The pH of slurries was adjusted to 3.5 by 0.1000M HNO_3 using a constant titration rate. For kaolinite and illite the slurries was slowly titrated with 0.0200M NaOH by titrator (Mettler Toledo**,** DL15) to 9.3-9.5 after more than two hours equilibrium at initial pH ~3.2. The corresponding titration rate of the base was set at a dE(mV) drift less than 5mV in 5min (dt). The more waiting time was choose for montmorillonite to achieve equilibrium. The montmorillonite slurry was adjusted to pH 3.2 by manually inject suitable HCl and equilibrium at 25°C at 100 rpm for four days before titration. Total proton concentration (TOTH) was calculated as following equation:

$$\mathrm{TOTH}=\frac{C_a V_a - C_b V_b}{V_0 + V_a + V_b} \qquad \text{Eq.1}$$

Here, C_a and C_b represent the concentrations of the standard acid and base solutions, respectively. V_a denotes the total volume of acid consumed during titration, while V_b corresponds to the cumulative volume of base added at each titration step. V_0 is the

initial volume of the clay slurries. The dilution factor (D) throughout the titration procedure was determined using the following equation:

$$D=\frac{V_0+V_a}{V_0+V_a+V_b} \quad \text{Eq.2}$$

The surface acidity constants were subsequently obtained by fitting three independent titration datasets using the FITEQL program (Westall 1979).

2.3 adsorption of phosphate on kaolinite, illite and montmorillonite

Dissolving 3.209 g of anhydrous sodium dihydrogen phosphate (Alfa Aesar) in 500 mL volumetric flask to obtain phosphate concentration of 53500 μmol/L. The concentration verification of solution was done and served as stock solution. The acid-treated and ion-exchanged clay samples were weighed and homogenized with 9 min ultrasonication method in 0.1, 0.01 and 0.001M KCl electrolyte solutions, which obtained the slurries of kaolinite, montmorillonite and illite with different ratios of solid/solution (15 g/L, 30 g/L and 7.5 g/L, respectively). 25mL homogenized slurries were took into 50 mL centrifuge tubes and initial pH values were adjusted with Hach HQ440d equipped with a PHC301 electrode by 1.0 and 0.1 M NaOH/HCl solutions. The electrode was calibrated using four standard buffer solutions with pH values of 1.68, 4.01, 7.00 and 9.18. 3.835 mL of the prepared working solution (535 μmol/L) was added into each centrifuge tube containing 25 mL clay suspension, resulting in the initial phosphate concentration of 84 μmol/L. The suspension was shaken at velocity of 100 rpm and 25 °C for 24 h. The supernatant was centrifuged at 10000 rpm (12000 × G) for 10 min, then filtered through a 0.45 μm membrane filter, and the phosphorus concentration in the solution was determined by Inductively Coupled Plasma Optical Emission Spectrometry (ICP-OES, iCAP6500 ThermoFisher). Each adsorption series was composed of 11 evaluation points within a pH range of 2.0 to 10.5. The adsorption of

PO_4 was calculated from the difference between the initially added, final concentrations of PO_4 in the equilibrium and bank solution (Only clay slurry) at same pH condition. Good dispersion of the samples and subtraction of the blank samples are essential prerequisites for obtaining reliable adsorption envelope data.

2.4 Constant Capacitance Model (CCM) and Triple Layer Model (TLM)

SCM can quantitatively relate adsorption behavior to solution chemistry and surface properties, and has been extensively applied to clay minerals, metal oxides, and environmental interfaces. In this study, both the Constant Capacitance Model (CCM) and Triple Layer Model (TLM) were employed to simulate the adsorption envelope behavior of phosphate on clay minerals. The CCM assumes that all surface reactions occur on a single surface plane and describes the electrostatic correction using a constant capacitance between the mineral surface and the bulk solution (Goldber and Sposito 1984a,b; Manning and Goldberg 1996; Nilsson et al. 1996; Nowack and Stone 2006). Unlike CCM, the TLM assumes that surface charge is distributed among the surface plane and two electrostatic planes, allowing a more realistic description of inner-sphere and outer-sphere surface complexes (Kanematsu et al. 2010). Model calculations were performed using the FITEQL software (Westall 1979), which optimizes surface complexation parameters through nonlinear least-squares fitting.

2.5 Attenuated total reflection-Fourier transform infrared spectroscopy (ATR-FTIR) analysis

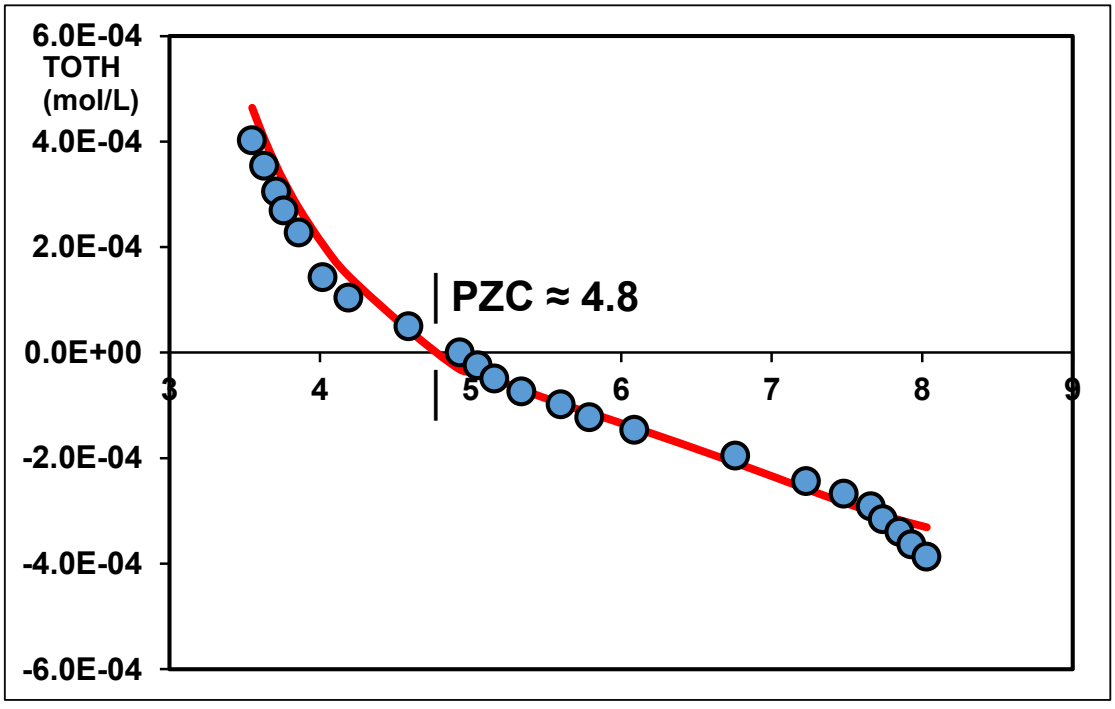
ATR-FTIR analysis of post-adsorption under the condition of maximum adsorption capacity for kaolinite, illite and montmorillonite were performed using a Perkin-Elmer Fourier Transform infrared spectrometer coupled with a diamond attenuated total reflection (ATR) accessory. Spectra were collected in a range of 400-4000 cm^{-1} with a spectral resolution of 1 cm^{-1} and 64 scans per sample. The adsorbed phosphate

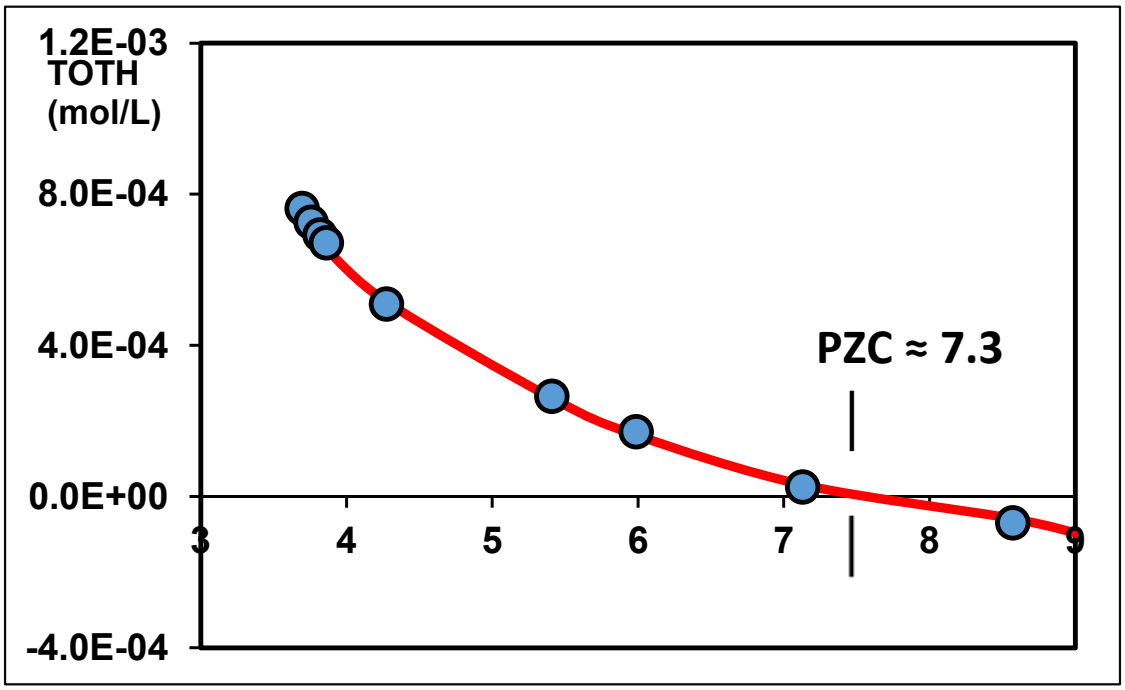
vibrations were analyzed based on reference data from Tejedor-Tejedor and Anderson (1990).

3. Result and discussion

3.1 determination of protonation and deprotonation constants

Although kaolinite, montmorillonite, and illite belong to the same class of layered silicate minerals, substantial differences were observed in their surface protonation and deprotonation constants. The Ka_1 and Ka_2 values were determined to be 4.61 and -6.68 for kaolinite, 9.31 and −5.12 for montmorillonite, and 6.12 and −7.46 for illite, respectively (Table1 and 2) . The BET specific surface areas of the ion-exchanged minerals were 20.8 m^2/g for kaolinite, 51.8 m^2/g for montmorillonite, and 36.4 m^2/g for illite. The PZC values decreased in the order of montmorillonite (7.3) > illite (6.5) > kaolinite (4.8) (Fig.1). Such variations may arise from differences in particle size distribution, the relative abundance of AlOH and SiOH surface functional groups, and variations in mineral treatment and experimental methodologies.




1.2E-03
TOTH
(mol/L)
8.0E-04
4.0E-04
0.0E+00
-4.0E-04
3
4
5
6
7
8
9
PZC ≈ 7.3

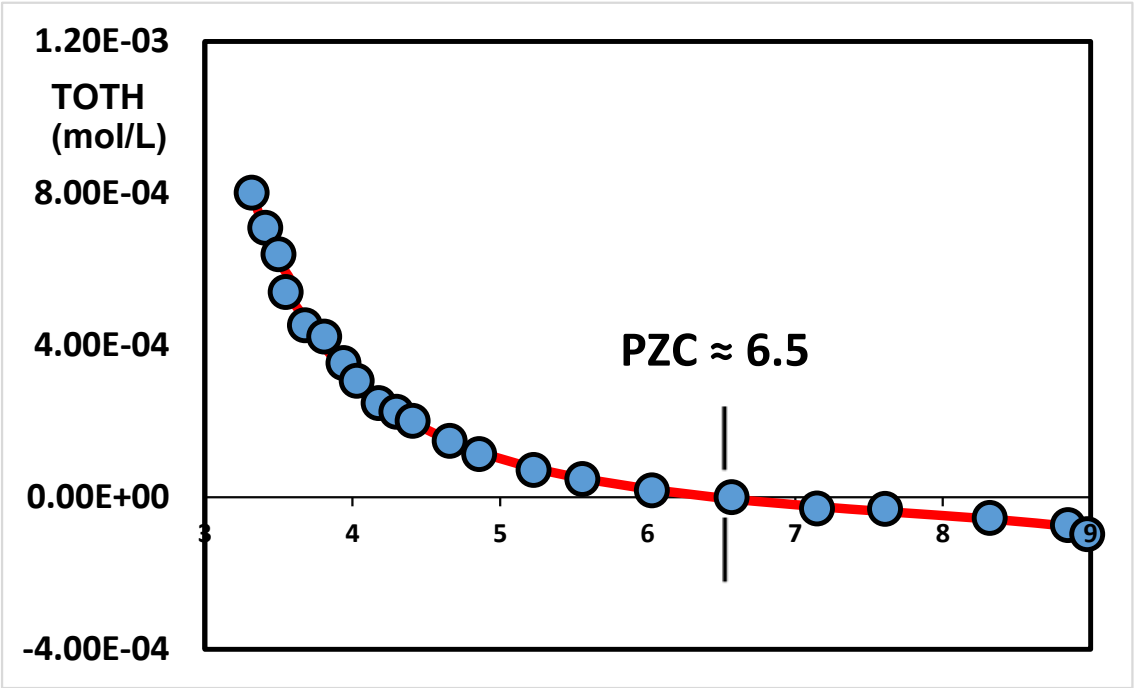
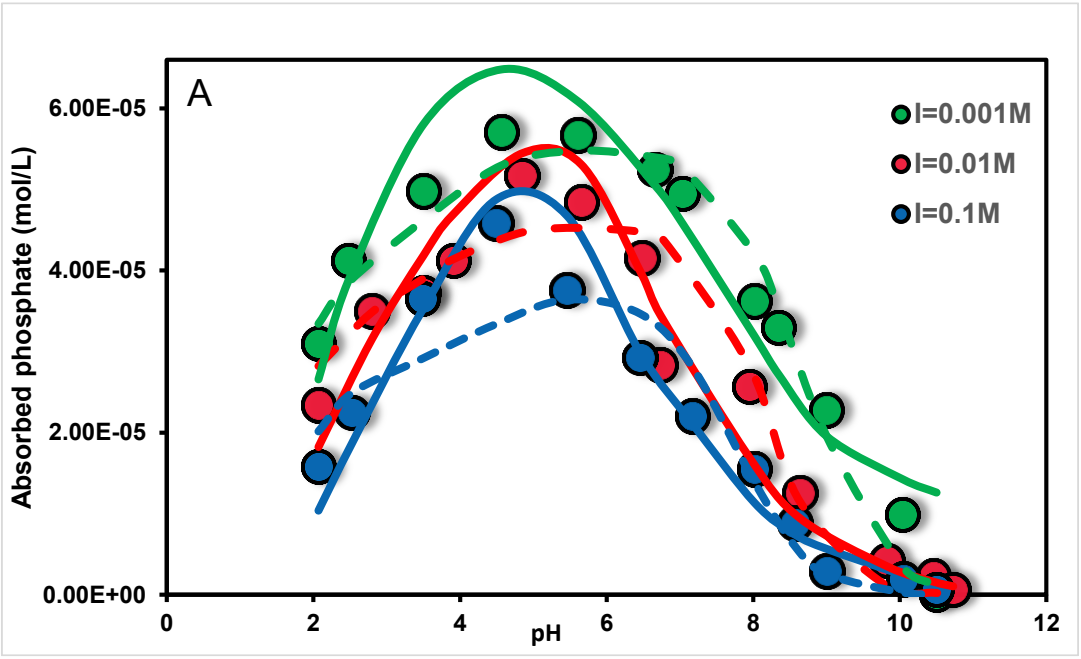
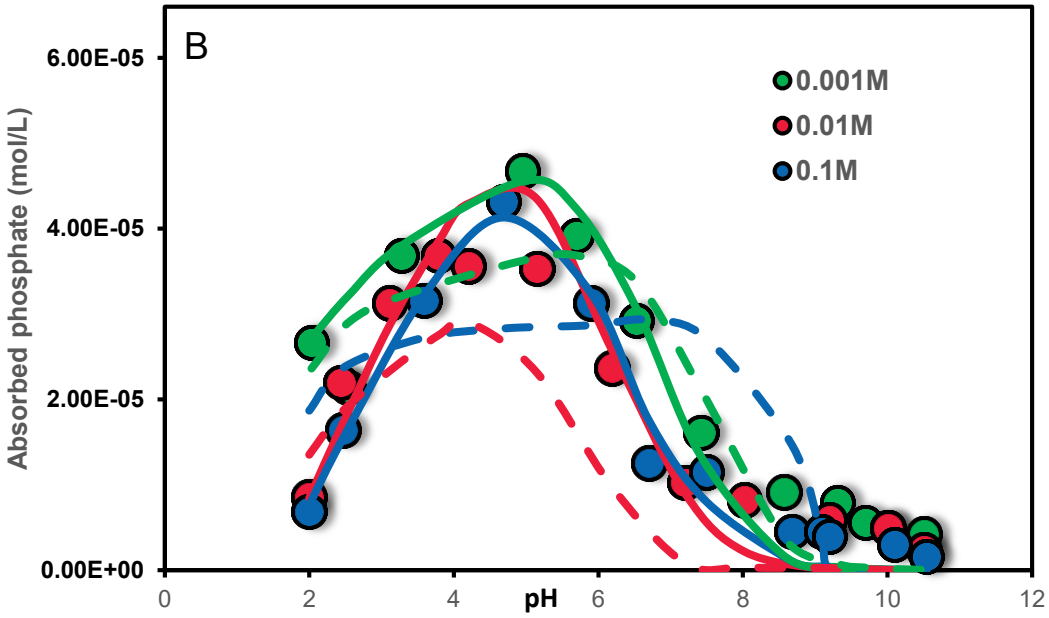

1.20E-03
TOTH
(mol/L)
8.00E-04
4.00E-04
0.00E+00
-4.00E-04
3
4
5
6
7
8
9
PZC ≈ 6.5

Fig. 1. Surface acid–base titration curves of kaolinite, montmorillonite, and illite. The solid concentrations were 15 g/L, 7.5 g/L, and 15 g/L, respectively, and the background electrolyte was 0.01 M $NaNO_3$.

3.2 Comparison of CCD and TLM model

Direct determination of surface site densities is challenging for clay-like minerals because of its heterogeneous surface structure, which comprises envelope-AlOH, envelope-SiOH, basal-AlOH, and permanent-charge sites and are different for iron oxides. Based on crystallographic considerations, permanent reactive site densities of 7.6 and 8.2 sites/nm² (envelope surface area basis) were proposed by Sposito (1984) and White and Zelazny (1988), respectively, whereas Wieland and Stumm (1992) obtained a value of 12.5 sites nm^{-2} by fitting acid–base titration data. Using the B-chain envelope-site model of White and Zelazny (1988), the corresponding envelope-site densities are 5.5 sites/nm² for AlOH groups and 2.7 sites/nm² for SiOH groups. Assuming that envelope surfaces account for approximately 10% of the total surface area, these values correspond to 0.55 and 0.27 sites/nm², respectively, when expressed on a total surface area basis. The corresponding surface parameters are given in table 3 and the model fits to the experimental data are shown in Figure 2. The optimized equilibrium constants based on the TLM for the $AlHPO_4^-$, $SiOH_2^+$–PO_4^{3-}, and $AlPO_4^{2-}$ surface complexes were 24.53, 18.60, and 17.44 for kaolinite, 23.68, 17.83, and 17.56 for montmorillonite, and 23.09, 19.51, and 17.23 for illite, respectively. Notably, the optimized log K values for the $AlPO_4^{2-}$ (17.44) and $SiOH_2^+$–PO_4^{3-} (18.60) surface complexes on kaolinite are in good agreement with those reported by He (1995).


A
6.00E-05
4.00E-05
2.00E-05
0.00E+00
Absorbed phosphate (mol/L)
0
2
4
6
8
10
12
pH
I=0.001M
I=0.01M
I=0.1M


B
6.00E-05
4.00E-05
2.00E-05
0.00E+00
Absorbed phosphate (mol/L)
0
2
4
6
8
10
12
pH
0.001M
0.01M
0.1M

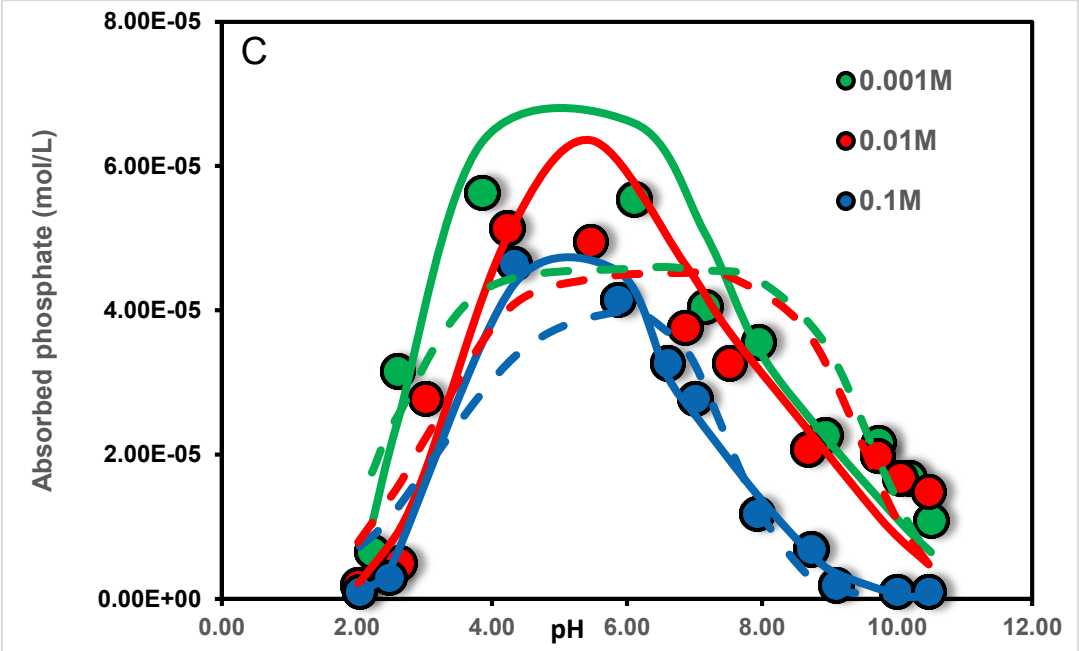


Fig.2 Adsorption envelope of phosphate on kaolinite (A), montmorillonite (B) and illite (C) in 0.001, 0.01 and 0.1 M KCl. The various color lines refer to the predicted adsorption envelope by surface complexation model (solid: TLM; dash: CCD). The SCM model with the parameters given in the table 1 and table 2.

Table 1 The parameters of kaolinite, montmorillonite and illite used in TLM modeling for $PO4^{3-}$

Property	Kaolinte		Montmorillonite		illite	
Surface area (m_2/g) †, S_A	20.77		51.80		36.40	
Cation Exchange Capacity (cmol/Kg)¶, CEC	3.6		9.1		6.4	
Site density (sites/nm^2)	AlOH	SiOH	AlOH	SiOH	AlOH	SiOH
	0.55	0.27	0.55	0.27	0.55	0.27
Solid concentration, Cs (g/L)	15		7.5		30	
Site concentration, N_t (mol/L)	3.66×10^{-4}	1.80×10^{-4}	4.56×10^{-4}	2.24×10^{-4}	1.28×10^{-4}	6.30×10^{-4}

† Measured based on BET method

¶ Measured based on Gu (2006)'s method

Table 2 reactions and equilibrium constants used in CCD modeling for PO_4^{3-} adsorption

Reaction	LogK
Equilibrium in aqueous phase	
$H_2O \rightleftharpoons H^- + OH^-$	14.00
$H+ + PO_4^{3-} \rightleftharpoons HPO_4^{2-}$	12.35
$2H+ + PO_4^{3-} \rightleftharpoons H_2PO_4^-$	19.55
$3H^+ + PO_4^{3-} \rightleftharpoons H_3PO4^0$	21.71
Surface protolysis	
$\equiv SOH^0 + H^+ \rightleftharpoons \equiv SOH_2^+$	K: 4.61 M: 6.12 I: 7.46
$\equiv SOH^0 \rightleftharpoons \equiv SO^- + H^+$	K: -6.68 M:-7.45 I: -5.12
Complexation of Electrolyte ion	
$\equiv X^-.H^+ + K^+ \rightleftharpoons \equiv X^-.K^+ + H^+$	-2.02 (Fit)
Surface complexation	Fit
$\equiv SOH + PO_4^{3-} + 3H^+ \rightleftharpoons \equiv SOH_2PO_4 + H_2O$	K: 29.13 M: 29.54 I: 28.30 (Fit)
$\equiv SOH + PO_4^{3-} + 2H^+ \rightleftharpoons \equiv SOHPO_4 + H_2O$	K: 25.62 M: 26.13 I: 24.83 (Fit)
$\equiv SOH + PO_4^{3-} + H^+ \rightleftharpoons \equiv SPO_4 + H_2O$	K: 17.84 M: 18.32 I: 16.87 (Fit)

Table 3 Reactions and equilibrium constants used in TLM modeling for PO_4^{3-} adsorption on kaolinite, montmorillonite and illite

Reaction	LogK

Equilibrium in aqueous phase		
$H_2O \rightleftharpoons H^- + OH^-$	14.00	
$H+ + SO_4^{2-} \rightleftharpoons HSO_4^-$	1.99	
$K+ + SO_4^{2-} \rightleftharpoons KSO_4^-$	0.85	
$H+ + PO_4^{3-} \rightleftharpoons HPO_4^{2-}$	12.35	
$2H+ + PO_4^{3-} \rightleftharpoons H_2PO_4^-$	19.55	
$3H^+ + PO_4^{3-} \rightleftharpoons H_3PO4^0$	21.71	
$K+ + H+ + PO_4^{3-} \rightleftharpoons KHPO_4^-$	12.64	
Surface protolysis		
$AlOH + H+ \rightleftharpoons AlOH_2^+$	7.89‡	
$AlOH \rightleftharpoons AlO^- + H^+$	-9.05‡	
$SiOH + H+ \rightleftharpoons SiOH_2^+$	2.00 §	
$SiOH \rightleftharpoons SiO^- + H^+$	-6.80 §	
Complexation of Electrolyte ion		
$AlOH + K^+ \rightleftharpoons AlO{-}K^+ + H^+$	-9.20 ¶	
$AlOH + H^+ + Cl^- \rightleftharpoons AlOH_2^+\text{-}Cl^-$	7.90 ¶	
$SiOH + K^+ \rightleftharpoons SiO^-\text{-}K^+ + H^+$	-3.50 #	
Inner-sphere complexes		
$AlOH + PO_4^{3-} + H+ \rightleftharpoons AlPO_4^{2-} + H_2O$	K: 17.44	M:17.56 I: 17.23
$AlOH + PO_4^{3-} + 2H^+ \rightleftharpoons AlHPO_4^- + H_2O$	K: 24.53	M: 23.68 I: 23.99
$AlOH + PO_4^{3-} + 2H^+ \rightleftharpoons AlOH_2^+\text{-}HPO_4^{2-}$	-	-

$SiOH + PO_4^{3-} + H^+ \rightleftharpoons SiOH_2^+\text{-}PO_4^{3-}$	K: 18.60 M: 17.83	I: 19.51

‡ Huang and Stumm， 1973

§ Xie and Walther, 1992

¶ James and Parks, 1982

Zachara et al, 1988

3.3 adsorption comparison

The maximum phosphate adsorption capacities of kaolinite, montmorillonite, and illite were 5.71×10^{-5}, 4.68×10^{-5}, and 5.63×10^{-5} mol/L, respectively. After normalization to mineral mass, montmorillonite exhibited the highest adsorption capacity (6.23×10^{-6} mol/g), followed by kaolinite (3.81×10^{-6} mol/g) and illite (1.88×10^{-6} mol/g). The normalized adsorption capacities of kaolinite and illite corresponded to 61.1% and 30.1% of that of montmorillonite, respectively. Changes in ionic strength exerted a moderate influence on phosphate adsorption. The differences between the minimum and maximum adsorption capacities were 19.8% for kaolinite, 21.2% for montmorillonite, and 17.6% for illite, indicating that montmorillonite was the most sensitive to ionic strength, whereas illite showed the weakest response.

3.4 effect of ionic strength

The phosphate adsorption envelopes showed that increasing ionic strength generally reduced the maximum adsorption capacity of all three clay minerals. For kaolinite, the maximum phosphate adsorption decreased from 5.71×10^{-5} mol/L at 0.001 M ionic strength to 4.58×10^{-5} mol/L at 0.1 M, corresponding to a reduction of 19.8%. For montmorillonite, the maximum adsorption decreased from 4.68×10^{-5} to 4.32×10^{-5} mol/L, representing a reduction of only 7.6%. For illite, the maximum adsorption decreased from 5.63×10^{-5} to 4.64×10^{-5} mol/L, corresponding to a reduction of 17.6%.

These results indicate that phosphate adsorption on kaolinite was most sensitive to changes in ionic strength, followed by illite, whereas montmorillonite exhibited the weakest ionic-strength dependence.

After normalization by the solid-to-solution ratio, the maximum adsorption capacities were calculated as 3.81×10^{-6} mol/g for kaolinite, 6.23×10^{-6} mol/g for montmorillonite, and 1.88×10^{-6} mol/g for illite. Therefore, the phosphate adsorption capacity on a mass basis followed the order: montmorillonite > kaolinite > illite. The normalized adsorption capacity of montmorillonite was approximately 3.3 times greater than that of illite, indicating a substantially higher affinity for phosphate per unit mass.

3.5 FTIR analysis of adsorbed phosphate

The characteristic phosphate vibrational bands on kaolinite were identified at 650, 960, 1027, and 1100 cm^{-1} (Fig. 3), which can be assigned to the ν_4, ν_1, and ν_3 phosphate stretching modes. A weak absorption feature at 936 cm^{-1} was also observed as a splitting of the ν_3 vibration. These band positions are in good agreement with previous studies reporting phosphate absorptions in the ranges of 935-960 cm^{-1} and 1015-1070 cm^{-1} (Kosugi and Ishiguro 2018; Jiao et al. 2019; Zhang et al. 2020; Garcia et al. 2021). The band centered at 1027 cm^{-1} has been attributed to monodentate phosphate complexes on mineral surfaces (Wu et al. 2022). Compared with kaolinite, the phosphate-related bands observed on montmorillonite and illite were much less intense. Nevertheless, the similarity in both band positions and spectral features suggests that phosphate was predominantly adsorbed as comparable inner-sphere surface complexes

on all three clay minerals.

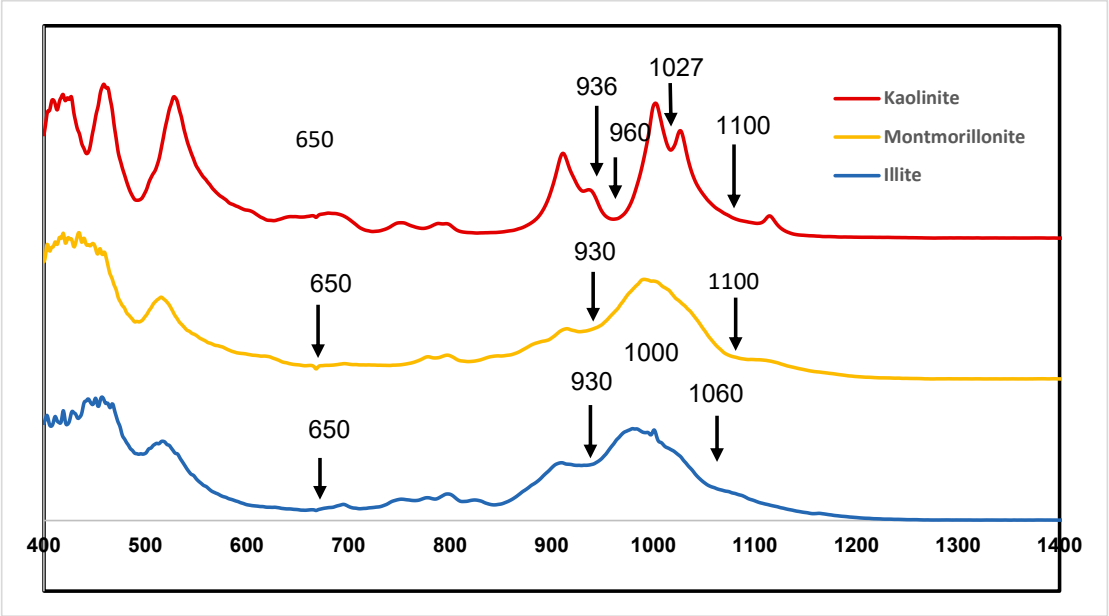


Fig. 3. ATR-FTIR spectra of phosphate-absorbed kaolinite, montmorillonite, and illite (initial pH = 4.85, 5.15, and 5.46, respectively).

3.6 Similarity comparison of phosphate envelopes

Comparison of adsorption-envelope curves provides additional insight into the differences in phosphate adsorption behavior among clay minerals and contributes to a better understanding of phosphate retention in soils containing mixed clay assemblages. In this study, the similarity between phosphate adsorption-envelope curves of kaolinite, montmorillonite, and illite was quantified using the Euclidean distance approach. For two adsorption-envelope curves represented by vectors A = (a_1, a_2...a_n) and B = (b_1, b_2...b_n), the Euclidean distance (d) was calculated as:

$$d=\sqrt{[\sum (a_i-b_i)]^2} \qquad \text{(Eq.1)}$$

where a_i and b_i denote the phosphate adsorption values corresponding to the same initial pH condition. A smaller Euclidean distance indicates a greater similarity between the two adsorption-envelope curves, whereas a larger distance reflects greater dissimilarity.

To facilitate comparison among different mineral pairs, a normalized similarity index (S) was further defined as:

$$SI=\exp(-kd) \quad \text{(Eq.2)}$$

where S is the similarity index, d is the Euclidean distance, and k is a scaling coefficient controlling the rate of similarity decay with increasing distance. The similarity index ranges from 0 to 1, with values approaching 1 indicating highly similar adsorption-envelope curves. Because the experimental pH values did not always coincide among different datasets, interpolation was applied to obtain adsorption values at identical initial pH points prior to distance calculation. The calculated similarity between kaolinite and illite was the highest (SI=0.47), followed by kaolinite and montmorillonite (SI=0.46), whereas montmorillonite and illite exhibited the lowest similarity (S = 0.34). The phosphate adsorption-envelope curves of kaolinite and illite were the most similar among the three clay minerals examined. In contrast, montmorillonite and illite exhibited the largest difference in adsorption behavior.

4. Conclusions

Kaolinite, montmorillonite, and illite were investigated through surface site titration and phosphate adsorption modeling. The major conclusions are summarized as follows.

The protonation (pK_{a1}) and deprotonation constants (pK_{a2}) of kaolinite, montmorillonite, and illite were determined to be 4.61 and -6.68 for kaolinite, 9.31 and -5.12 for montmorillonite, and 6.12 and -7.46 for illite, respectively. Due to their different adsorption capacities, different solid-to-solution ratios were employed in this study. After normalization, the maximum phosphate adsorption capacities under the same initial phosphate concentration were calculated to be 3.81×10^{-6} mol/g for kaolinite, 6.23×10^{-6} mol/g for montmorillonite, and 1.88×10^{-6} mol/g for illite. An increase in ionic

strength reduced phosphate adsorption, with the maximum adsorption capacity decreasing by up to 19.8% for kaolinite, 17.6% for illite, and 7.6% for montmorillonite.

Compared with the Constant Capacitance Model (CCM), the Triple Layer Model (TLM) provided a substantially better fit to the phosphate adsorption envelope data. The recommended surface complexation constants of phosphate ($AlHPO_4^-$, $SiOH_2^+$–PO_4^{3-}, and $AlPO_4^{2-}$) were 24.53, 18.60, and 17.44 for kaolinite, 23.68, 17.83, and 17.56 for montmorillonite, and 23.09, 19.51, and 17.23 for illite, respectively. Similarity analysis of the adsorption envelopes indicated that the phosphate adsorption behavior of kaolinite was more similar to that of illite, whereas montmorillonite exhibited distinctly different adsorption characteristics. ATR-FTIR spectra of the phosphate-adsorbed samples revealed four major absorption bands located at approximately 650, 960, 1027, and 1100 cm^{-1}. These bands were assigned to the ν_4, ν_1, and ν_3 phosphate stretching vibrations. The identical positions and number of these absorption bands among the three minerals suggest that phosphate was adsorbed in same surface complexation forms on kaolinite, montmorillonite, and illite.

Statements and Declarations

Funding

This work was supported by the Sichuan Province Science and Technology Support Program (2024ZYD0042).

Competing Interests

The authors declare that they have no competing interests.

Author Contributions

Ying HUANG: Writing – original draft, review & editing, Data curation, Visualization, Validation, Methodology, Investigation, Funding acquisition, Conceptualization.

Jing LIU: Writing – review & editing, Visualization, Funding acquisition, Project administration, Resource.

Ethics Approval

This is not applicable.

Consent to Publish

This is not applicable.

Data Availability

The data supporting the findings of this study are available from the corresponding author upon reasonable request.

Acknowledgements

We gratefully acknowledge Prof. Yun-Gui Li of Southwest University of Science and Technology for providing the FITEQL user manual and Prof. Weiqing Wang for valuable discussions and insights regarding the modeling.

References

Abollino, O., Giacomino, A., Malandrino, M., Mentasti, E., 2008. Interaction of metal ions with montmorillonite and vermiculite. Applied Clay Science 38, 227–236. https://doi.org/10.1016/j.clay.2007.04.002

Berg, A.S., Joern, B.C., 2006. Sorption dynamics of organic and inorganic phosphorus compounds in soil. Journal of Environmental Quality 35, 1855–1862. https://doi.org/10.2134/jeq.2005.0420

Brady, N.C., Weil, R.R., 2002. The Nature and Properties of Soils, 13th ed. Prentice Hall, Upper Saddle River, NJ.

Dalal, R.C., 1977. Soil organic phosphorus. Advances in Agronomy 29, 83-117. https://doi.org/10.1016/S0065-2113(08)60216-3

Davis, J.A., Kent, D.B., 1990. Surface complexation modeling in aqueous geochemistry. In: Hochella, M.F., White, A.F. (Eds.), Mineral-Water Interface Geochemistry. Mineralogical Society of America, Washington, DC, pp. 177-258.

Dzombak, D.A., Morel, F.M.M., 1990. Surface Complexation Modeling: Hydrous Ferric Oxide. Wiley-Interscience, New York.

Garcia K I , Quezada G R ,Arumi, Jose L.Urrutia, RobertoToledo, Pedro G.Ad sorption of Phosphate Ions on the Basal and Edge Surfaces of Kaolinite in Lo w Salt Aqueous Solutions Using Molecular Dynamics Simulations[J].The journa l of physical chemistry, C. Nanomaterials and interfaces, 2021, 125(38):21179-2 1190.DOI:10.1021/acs.jpcc.1c05995.

Gauthier, J., 2011. Modeling the adsorption of phosphate in agricultural soils of southern Ontario. Ph.D Thesis. University of Guelph, Guelph, Ontario, Canada.

Goldberg, S. Sposito, G. 1984a. A Chemical Model of Phosphate Adsorption by Soils: I. Reference Oxide Minerals. Soil Science Society of America Journal 48(4), 772–778. https://doi.org/10.2136/sssaj1984.03615995004800040015x.

Goldberg, S. Sposito, G. 1984b. A Chemical Model of Phosphate Adsorption b y Soils: II. Noncalcareous Soils. Soil Science Society of America Journal 48 (4), 779–783. https://doi.org/10.2136/sssaj1984.03615995004800040016x.

Goldberg, S., 1985. Chemical modeling of anion adsorption on soil constituent s. Ph.D. Dissertation. University of California, Riverside, CA, USA.

Goldberg, S., 2014. Application of surface complexation models to anion adsor ption by natural materials.Environmental Toxicology and Chemistry 33, 2172–21 80. https://doi.org/10.1002/etc.2687

Goldberg, S., Criscenti, L.J., 2008. Modeling adsorption of metals and metalloids by soil components. In: Violante, A., Huang, P.M., Gadd, G.M. (Eds.), Biophysico-Chemical Processes of Heavy Metals and Metalloids in Soil Environments. John Wiley & Sons, Hoboken, NJ, pp. 216-264.

Gu, X.Y., 2006. Surface complexation modelling of heavy metal adsorption on natural clay minerals. Ph.D. Dissertation. University of Guelph, Guelph, Ontario, Canada.

He L.M. 1995. Adsorption of sulfate and phosphate at the mineral water interface: isotherm, stoichimiometry and omdels. Ph.D dissertation, The Virginia Polytechnic Institute and State University. 1-186.

Huang, C.P., Stumm, W., 1973. Specific adsorption of cations on hydrous γ-Al_2O_3. Journal of Colloid and Interface Science 43, 409-420. https://doi.org/10.1016/0021-9797(73)90391-3

James, R.O., Parks, G.A., 1982. Characterization of aqueous colloids by their electrical double-layer and intrinsic surface chemical properties. In: Matijević, E. (Ed.), Surface and Colloid Science, Vol. 12. Plenum Press, New York, pp. 119-216.

Jiao, Y., Wang, X., Zhao, Q., Zhang, Y., Liu, J., Chen, H., 2019.Effects of phosphate-solubilizing bacteria on phosphorous release and sorption on montmorillonite. Applied Clay Science 181, 105227. https://doi.org/10.1016/j.clay.2019.105227

Kanematsu, M., Young, T.M., Fukushi, K., Green, P.G., Darby, J.L. 2010. Extend triple layer modeling of arsenate and phosphate adsorption on a goethite-based granular porous adsorbent. Environment Science and Technology 44, 3388-3394.

Kosugi, S., Ishiguro, M., 2018. Phosphate adsorption properties and modeling o f Iriki kaolinite. Journal of the Japanese Society of Irrigation, Drainage and Ru ral Engineering 86(1), I_63-I_70. https://doi.org/10.11408/jsidre.86.I_63

Levesque, M., Schnitzer, M., 1967. The extraction of soil organic matter by ba se and chelating resin. Canadian Journal of Soil Science 47, 76-78. https://doi.o rg/10.4141/cjss67-012

Manning, B. A. Goldberg, S. 1996. Modeling Arsenate Competitive Adsorption on Kaolinite, Montmorillonite and Illite. Clays and Clay Minerals 44(5), 609–6 23. https://doi.org/10.1346/CCMN.1996.0440504.

Miranda-Trevino, J.C., Coles, C.A., 2003. Kaolinite properties, structure and infl uence of metal retention on pH. Applied Clay Science 23, 133–139. https://doi. org/10.1016/S0169-1317(03)00095-4.

Nilsson, N. Persson, P. Lövgren, L. Sjöberg, S. 1996. Competitive surface com plexation of o-phthalate and phosphate on goethite (α-FeOOH) particles. Geochi mica et Cosmochimica Acta 60(22), 4385–4395. https://doi.org/10.1016/S0016-70 37(96)00258-X.

Nowack, B. Stone, A. T. 2006. Competitive adsorption of phosphate and phosphonates onto goethite. Water Research, 40(11), 2201–2209. https://doi.org/10.1016/j.watres.2006.03.018.

Perrott, K.W., Sarathchandra, S.U., Waller, J.E., 1990. Seasonal storage and release of phosphorus and potassium by organic matter and the microbial biomass in a high-producing pastoral soil. Australian Journal of Soil Research 28, 593-608. https://doi.org/10.1071/SR9900593

Schoonheydt, R.A., Johnston, C.T., Bergaya, F., 2018. Clay minerals and their surfaces. In: Bergaya, F., Lagaly, G. (Eds.), Surface and Interface Chemistry of Clay Minerals. Developments in Clay Science, Vol. 9. Elsevier, Amsterdam, pp. 1–21. https://doi.org/10.1016/B978-0-08-102432-4.00001-9.

Sposito, G., 1984. The Surface Chemistry of Soils. Oxford University Press, New York.

Stewart, J.W.B., Tiessen, H., 1987. Dynamics of soil organic phosphorus. Biogeochemistry 4, 41-60. https://doi.org/10.1007/BF02187361

Tejedor-Tejedor, M.I., Anderson, M.A., 1990. Protonation of phosphate on the surface of goethite as studied by CIR-FTIR and electrophoretic mobility. Langmuir 6, 602–611. https://doi.org/10.1021/la00093a015

Westall, J.C., 1979. FITEQL: A computer program for determination of chemic al equilibrium constants from experimental data. Version 1.0. Report 79-01, De partment of Chemistry, Oregon State University, Corvallis, OR.

White, G.N., Zelazny, L.W., 1988. Analysis and implications of the edge struct ure of dioctahedral phyllosilicates. Clays and Clay Minerals 36, 141-146. https:/ /doi.org/10.1346/CCMN.1988.0360207

Wieland, E., Stumm, W., 1992. Dissolution kinetics of kaolinite in acidic aqueo us solutions at 25°C. Geochimica et Cosmochimica Acta 56, 3339-3355. https:// doi.org/10.1016/0016-7037(92)90312-7

Wu, Q., Chen, J., Ren, Y., Du, Y., Wang, S., Zhang, D., Liao, J., Wang, X. (2 022). Species identification of phosphate at the ZrO_2/water interface: A combin ed ATR-FTIR and DFT study. Applied Surface Science, 606, 154946. https://d oi.org/10.1016/j.apsusc.2022.154946

Xie, Z., Walther, J.V., 1992. Incongruent dissolution and surface area of kaolini te. Geochimica et Cosmochimica Acta 56, 3357-3363. https://doi.org/10.1016/00 16-7037(92)90313-8

Zachara, J.M., Cowan, C.E., Schmidt, R.L., Ainsworth, C.C., 1988. Chromate a dsorption by kaolinite. Clays and Clay Minerals 36, 317-326. https://doi.org/10. 1346/CCMN.1988.0360406

Zhang, H., Elskens, M., Chen, G., Snoeck, C., Chou, L., 2020. Influence of se awater ions on phosphate adsorption at the surface of hydrous ferric oxide (HF O). Science of the Total Environment 721, 137826. https://doi.org/10.1016/j.scito tenv.2020.137826